Int. J. Heat Mass Transfer. Vol. 36, No. 17, pp. 4173–4180, 1993
Printed in Great Britain

0017–9310/93 $6.00 + 0.00

Three-dimensional linear stability of natural convective flow between concentric horizontal cylinders

JUN YOUNG CHOI and MOON-UHN KIM

Department of Mechanical Engineering, Korea Advanced Institute of Science and Technology, 373-1, Kusong-dong, Yusung-gu, Taejon 305-701, Korea

(*Received* 25 *February* 1993 *and in final form* 13 *May* 1993)

Abstract—Linear stability of natural convective flow in an annulus between two concentric horizontal cylinders is studied numerically. In the medium-sized annulus with relative inverse gap ratio (ratio of inner diameter to gap width) between 2.1 and 10.0, the basic two-dimensional flow is found to be unstable with respect to three-dimensional disturbances. Critical Rayleigh numbers above which the two-dimensional basic flow is unstable show good agreement with experimental results. The disturbance velocity distribution obtained by the stability analysis suggests that the instability is mainly caused by buoyancy effects.

1. INTRODUCTION

NATURAL convection in an annulus between two horizontal concentric cylinders has attracted considerable attention because of its theoretical importance and wide technical applications including thermal storage and transmission systems. Extensive surveys on this configuration have been given by Kuehn and Goldstein [1], and recently by Fant *et al.* [2].

In an experimental investigation on characteristics of convecive flow of air in a horizontal annulus, Powe *et al.* [3] have presented a comprehensive description of different flow regimes depending on the Rayleigh number and gap width. Steady unicellular two-dimensional flow is observed at low values of the Rayleigh number. As the Rayleigh number is increased above a critical value, different unsteady flow patterns are found to occur depending on gap width: two-dimensional oscillatory pattern for a wide gap (inverse relative gap width σ being smaller than 2.8), three-dimensional spiral flow for a moderate gap ($2.8 < \sigma < 8.5$) and multicellular flow for a narrow gap ($\sigma > 8.5$). For a wide gap, unsteady crescent-shaped flow oscillating about the horizontal axis of cylinders appears when the Rayleigh number exceeds a critical value about 10^5. A detailed description of two-dimensional oscillatory pattern is given in ref. [4]. For a narrow gap, the two-dimensional multicellular flow consisting of one or more pairs of small counter-rotating cells in the top region of the inner cylinder occurs. However, the critical value obtained from experimental observations [3, 5] shows substantial discrepancy. In an annulus with moderate gap, flow pattern of three-dimensional spiral nature has been observed for Rayleigh number larger than about 1800. Experimental results, quoted in refs. [3, 6], as to the point at which the unicellular convection becomes unstable show reasonably good agreement. However, Grigull and Hauf [7] have reported that the spiral flow is observed even in a wide gap annulus, $\sigma > 2.08$.

Numerical computations [8, 9] confirm the transition to two-dimensional multi-cellular flow between narrow horizontal annulus for air at high Rayleigh number. The transition Rayleigh number, however, shows some discrepancy. Although several authors [8, 10, 11] have carried out numerical investigations on the three-dimensional convective flow, except for ref. [8], they consider the steady convection in a wide gap annulus and find that nearly two-dimensional crescent eddies establish in the central region and that the fluid particle moves along a coaxial double helix. Rao *et al.* [8], on the other hand, have confirmed the steady three-dimensional spiral convection occurs in a moderate gap for a fluid of high Prandtl number ($Pr = 5000$).

In this study, in an attempt to predict the critical Rayleigh number above which a three-dimensional spiral flow manifests and to obtain a clearer understanding of the spiral convection, we examine systematically the linear stability of steady two-dimensional (unicellular) convection of air ($Pr = 0.71$) in an annulus of medium-sized gap ($2.0 \leqslant \sigma \leqslant 10.0$) against three-dimensional disturbances. The basic two-dimensional velocity and temperature fields are obtained numerically, from lack of analytical expressions valid for a high Rayleigh number convection.

To study the stability of steady two-dimensional convection, each variable in the governing equations is decomposed in the form

$$q(r, \phi, z, t) = Q_s(r, \phi) + \varepsilon q_p(r, \phi, z, t), \quad \varepsilon \ll 1 \tag{1}$$

$$q_p(r, \phi, z, t) = \mathrm{Re}\,[\hat{q}(r, \phi, t) \exp(ikz)], \tag{2}$$

where Q_s denotes the basic flow and q_p the pertur-

NOMENCLATURE

b	buoyancy force
E	kinetic energy
g	gravitational acceleration
k	axial wave number
k	unit vector in axial direction
L	gap width of the annulus, $R_o - R_i$
Pr	Prandtl number, ν/α
Ra	Rayleigh number, $g\beta(T_i - T_o)L^3/\alpha\nu$
Re	real part of complex number
R_i, R_o	radii of the inner and outer cylinders, respectively
r	dimensionless radial coordinate
s	complex growth rate, $s_r + is_i$
t	dimensionless time
V	velocity for basic flow, $(V_r, V_\phi, 0)$
v	velocity
z	dimensionless axial coordinate.

Greek symbols

α	thermal diffusivity
β	thermal expansion coefficient
Θ	temperature for basic flow
θ	temperature
ν	kinematic viscosity
σ	inverse relative gap width, $2R_i/L$
ϕ	azimuthal coordinate
Ψ	stream function for basic flow
ψ	vector potential
ω	vorticity
Ω	vorticity for basic flow.

Subscripts

r, ϕ, z	radial, azimuthal and axial coordinates
c	critical value
i	inner cylinder
o	outer cylinder
s	two-dimensional steady basic flow solution
p	perturbation.

bation. Expression (2) in which the perturbation is assumed to vary sinusoidally in the axial direction is inferred from the method of normal mode [12], owing to the two-dimensionality of basic flow. Inserting equations (1) and (2) into governing equations, subtracting the basic flow and neglecting terms $O(\varepsilon^2)$ and higher, we obtain two-dimensional linear evolution equations for $\hat{q}$ with the axial wave number k as a parameter. The resulting equations for $\hat{q}$ are solved by time-marching integration under suitably chosen initial conditions. After a sufficiently long time, the solution of the initial value problem for the perturbation $\hat{q}(r, \phi, t)$ will approach the most unstable mode of the eigenvalue problem (which is independent of initial conditions) resulting from the usual normal mode analysis for the linearized disturbance equations:

$$\hat{q}(r, \phi, t) \sim \tilde{q}(r, \phi)\exp(st), \quad s = s_r + is_i \quad \text{as } t \to \infty, \tag{3}$$

from which we can infer the growth rate s_r and the frequency s_i of the most unstable mode.

In the present study, the problem is formulated in terms of vector potential, vorticity and temperature, and calculations are carried out by using the finite difference method. The formulation has advantages in that the equation of continuity is automatically satisfied and that the pressure distribution need not be obtained. Computations are carried out in the ranges of $10^3 \leqslant Ra \leqslant 10^5$ and $2.0 \leqslant \sigma \leqslant 10.0$ for a fluid of Prandtl number 0.71 (air). The critical Rayleigh numbers determined from the linear stability analysis show fairly good agreement with experimental results on the transition to the three-dimensional spiral convective flow presented in Powe *et al.* [3].

2. MATHEMATICAL FORMULATION AND COMPUTATIONAL METHOD

Laminar natural convective flow in an infinite horizontal annulus between two concentric circular cylinders with inner and outer radii R_i and R_o is considered. Figure 1 shows the geometrical model and the cylindrical coordinte system (r, ϕ, z), angular coordinate ϕ being measured counterclockwise from the upward vertical plane through the axis of cylinders. The inner and outer cylinder surfaces are maintained at different uniform temperatures T_i and T_o $(T_i > T_o)$. Adopting the Boussinesq approximation of neglecting the variations in physical properties, except for the density in the buoyancy terms, and introducing the vector potential ψ such that

$$\mathbf{v} = \nabla \times \psi, \tag{4}$$

the dimensionless governing equations are written [13] as

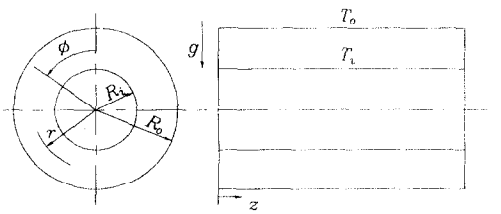

FIG. 1. Flow geometry and coordinates system.

$$\frac{\partial \boldsymbol{\omega}}{\partial t} + (\mathbf{v}\cdot\nabla)\boldsymbol{\omega} = (\boldsymbol{\omega}\cdot\nabla)\mathbf{v} + Pr\,\nabla^2\boldsymbol{\omega} + Ra\,Pr\,\nabla\times\mathbf{b} \quad (5)$$

$$\nabla^2\boldsymbol{\psi} = -\boldsymbol{\omega} \quad (6)$$

$$\frac{\partial\theta}{\partial t} + (\mathbf{v}\cdot\nabla)\theta = \nabla^2\theta, \quad (7)$$

where $\boldsymbol{\omega}$ is the vorticity, $\mathbf{b} = (\theta\cos\phi,\ -\theta\sin\phi,\ 0)$ the buoyancy force, θ the temperature. The vorticity transport equation (5) has been obtained by taking curl of the Navier–Stokes equations. Note that the equation of continuity is satisfied identically and that explicit appearance of the pressure is avoided. The dimensionless parameters Ra and Pr are defined as

$$Ra = g\beta(T_i - T_o)L^3/\alpha\nu, \quad Pr = \nu/\alpha, \quad (8)$$

where g is the acceleration due to gravity, β the thermal expansion coefficient, L the gap width $(R_o - R_i)$, α the thermal diffusivity and ν the kinematic viscosity. Equations (5)–(7) have been put into dimensionless form by taking L, L^2/α, α/L as characteristic length, time and velocity, respectively. Dimensionless temperature θ is defined by $\theta = (T - T_o)/(T_i - T_o)$.

The boundary conditions on rigid boundaries are expressed as [14]

$$\left.\begin{aligned} v_r = v_\phi = v_z = 0 \\ \partial(r\psi_r)/\partial r = \psi_\phi = \psi_z = 0 \\ \omega_r = 0, \quad \omega_\phi = -\partial v_z/\partial r, \quad \omega_z = \partial v_\phi/\partial r \end{aligned}\right\} \quad \text{at } r = r_i, r_o \quad (9)$$

$$\theta = 1 \quad \text{at } r = r_i \quad \text{and} \quad \theta = 0 \quad \text{at } r = r_o \quad (10)$$

where r_i and r_o are dimensionless radii of inner and outer cylinders, respectively.

2.1. *Two-dimensional basic flow equations*

For two-dimensional flow, the above equations (5)–(7) degenerate into the conventional vorticity–stream function formulation, by letting the z component of velocity equal to zero and all the variables be independent of z:

$$\mathbf{v} = \mathbf{V}(r,\phi,t) = (V_r, V_\phi, 0)$$
$$\boldsymbol{\omega} = \Omega(r,\phi,t)\mathbf{k}$$
$$\boldsymbol{\psi} = \Psi(r,\phi,t)\mathbf{k}$$
$$\theta = \Theta(r,\phi,t),$$

where $\mathbf{k}$ denotes the unit vector along the z-axis.

The dimensionless governing equations for two-dimensional convective flow are given as

$$\frac{\partial\Omega}{\partial t} + V_r\frac{\partial\Omega}{\partial r} + V_\phi\frac{\partial\Omega}{r\partial\phi} = Pr\,\nabla^2\Omega - Ra\,Pr\left(\frac{\partial\Theta}{\partial r}\sin\phi + \frac{\partial\Theta}{r\partial\phi}\cos\phi\right) \quad (11)$$

$$\nabla^2\Psi = -\Omega \quad (12)$$

$$V_r = \frac{\partial\Psi}{r\partial\phi}, \quad V_\phi = -\frac{\partial\Psi}{\partial r} \quad (13)$$

$$\frac{\partial\Theta}{\partial t} + V_r\frac{\partial\Theta}{\partial r} + V_\phi\frac{\partial\Theta}{r\partial\phi} = \nabla^2\Theta. \quad (14)$$

Boundary conditions on the cylinder surfaces are written as follows:

$$\Psi = 0, \quad \Omega = -\frac{\partial^2\Psi}{\partial r^2}, \quad \Theta = 1, \quad \text{at } r = r_i \quad (15)$$

$$\Psi = 0, \quad \Omega = -\frac{\partial^2\Psi}{\partial r^2}, \quad \Theta = 0, \quad \text{at } r = r_o. \quad (16)$$

After a sufficiently large time, the velocity and temperature fields satisfying equations (11)–(14) approach steady states for Rayleigh numbers in the range considered in the present work $(10^3 \leqslant Ra \leqslant 10^5)$.

2.2. *Linear stability formulation*

The stability of the basic two-dimensional steady convective flow to small disturbances is investigated, following the standard methods of linear stability theory [12]. We decompose the perturbed flow into the form:

$$\begin{aligned} \mathbf{v} &= \mathbf{V}_s(r,\phi) + \varepsilon\mathbf{v}_p(r,\phi,z,t) \\ \boldsymbol{\omega} &= \Omega_s(r,\phi)\mathbf{k} + \varepsilon\omega_p(r,\phi,z,t) \\ \boldsymbol{\psi} &= \Psi_s(r,\phi)\mathbf{k} + \varepsilon\psi_p(r,\phi,z,t) \\ \theta &= \Theta_s(r,\phi) + \varepsilon\theta_p(r,\phi,z,t), \end{aligned} \quad (17)$$

where subscripts s and p represent the basic steady flow and the perturbation, respectively. Hereafter, we delete the subscripts s and p for brevity. Inserting expressions (17) into equations (5)–(7), subtracting the basic steady part and discarding $O(\varepsilon^2)$ and higher order terms, we obtain a system of linear equations for the perturbations. Since the equations are linear and do not depend explicitly on z, we can assume the sinusoidal variation in the z-direction. Further, taking into consideration the reflectional symmetry in z $(z \to -z,\ v_r \to v_r,\ v_\phi \to v_\phi,\ v_z \to -v_z,\ \theta \to \theta)$, we write the perturbation as

$$\begin{cases} v_r = \hat{v}_r(r,\phi,t)\cos kz \\ v_\phi = \hat{v}_\phi(r,\phi,t)\cos kz \\ v_z = \hat{v}_z(r,\phi,t)\sin kz \\ \theta = \hat{\theta}(r,\phi,t)\cos kz \end{cases}$$

$$\begin{cases} \omega_r = \hat{\omega}_r(r,\phi,t)\sin kz \\ \omega_\phi = \hat{\omega}_\phi(r,\phi,t)\sin kz \\ \omega_z = \hat{\omega}_z(r,\phi,t)\cos kz \end{cases} \quad \begin{cases} \psi_r = \hat{\psi}_r(r,\phi,t)\sin kz \\ \psi_\phi = \hat{\psi}_\phi(r,\phi,t)\sin kz, \\ \psi_z = \hat{\psi}_z(r,\phi,t)\cos kz \end{cases} \quad (18)$$

where k is the dimensionless axial wave number. Factoring out the axial(z-) dependency, the final form of the linearized disturbance equations in which the axial wave number k appears as a parameter is given as follows (dropping the circumflex ^):

$$\frac{\partial \omega_r}{\partial t} + V_r \frac{\partial \omega_r}{\partial r} + V_\phi \frac{\partial \omega_r}{r\partial \phi} = \omega_r \frac{\partial V_r}{\partial r} + \omega_\phi \frac{\partial V_r}{r\partial \phi} - k\Omega_z v_r + Pr\left(\nabla_*^2 \omega_r - \frac{\omega_r}{r^2} - \frac{2}{r^2}\frac{\partial \omega_\phi}{\partial \phi}\right) - Ra\, Pr\, k\theta \sin\phi \quad (19a)$$

$$\frac{\partial \omega_\phi}{\partial t} + V_r \frac{\partial \omega_\phi}{\partial r} + V_\phi \frac{\partial \omega_\phi}{r\partial \phi} + \frac{V_\phi \omega_r}{r} = \omega_r \frac{\partial V_\phi}{\partial r} + \omega_\phi \frac{\partial V_\phi}{r\partial \phi} + \frac{\omega_\phi V_r}{r} - k\Omega_z v_\phi + Pr\left(\nabla_*^2 \omega_\phi - \frac{\omega_\phi}{r^2} + \frac{2}{r^2}\frac{\partial \omega_r}{\partial \phi}\right) - Ra\, Pr\, k\theta \cos\phi \quad (19b)$$

$$\frac{\partial \omega_z}{\partial t} + v_r \frac{\partial \Omega_z}{\partial r} + V_r \frac{\partial \omega_z}{\partial r} + v_\phi \frac{\partial \Omega_z}{r\partial \phi} + V_\phi \frac{\partial \omega_z}{r\partial \phi} = k\Omega_z v_z + Pr\, \nabla_*^2 \omega_z - Ra\, Pr\left(\frac{\partial \theta}{\partial r}\sin\phi + \frac{\partial \theta}{r\partial \phi}\cos\phi\right) \quad (19c)$$

$$\nabla_*^2 \psi_r - \frac{\psi_r}{r^2} - \frac{2}{r^2}\frac{\partial \psi_\phi}{\partial \phi} = -\omega_r \quad (20a)$$

$$\nabla_*^2 \psi_\phi - \frac{\psi_\phi}{r^2} + \frac{2}{r^2}\frac{\partial \psi_r}{\partial \phi} = -\omega_\phi \quad (20b)$$

$$\nabla_*^2 \psi_z = -\omega_z \quad (20c)$$

$$v_r = \frac{\partial \psi_z}{r\partial \phi} - k\psi_\phi \quad (21a)$$

$$v_\phi = -\frac{\partial \psi_z}{\partial r} + k\psi_r \quad (21b)$$

$$v_z = \frac{\partial (r\psi_\phi)}{r\partial r} - \frac{\partial \psi_r}{r\partial \phi} \quad (21c)$$

$$\frac{\partial \theta}{\partial t} + v_r \frac{\partial \Theta}{\partial r} + V_r \frac{\partial \theta}{\partial r} + v_\phi \frac{\partial \Theta}{r\partial \phi} + V_\phi \frac{\partial \theta}{r\partial \phi} = \nabla_*^2 \theta, \quad (22)$$

where

$$\nabla_*^2 = \frac{\partial^2}{\partial r^2} + \frac{\partial}{r\partial r} + \frac{1}{r^2}\frac{\partial^2}{\partial \phi^2} - k^2.$$

The boundary conditions are

$$\left.\begin{aligned} &v_r = v_\phi = v_z = \partial(r\psi_r)/\partial r = \psi_\phi = \psi_z = \theta = 0 \\ &\omega_r = 0, \quad \omega_\phi = -\partial v_z/\partial r, \quad \omega_z = \partial v_\phi/\partial r \end{aligned}\right\} \quad \text{at } r = r_i, r_o. \quad (23)$$

Since the above linear disturbance equations are homogeneous and do not depend on t explicitly, the solution will eventually show the exponential behavior in time:

$$q(r, \phi, t) \sim \tilde{q}(r, \phi)\, e^{st}, \quad s = s_r + is_i \quad t \gg 1, \quad (24)$$

where $\tilde{q}$ denotes the most unstable (least stable) mode of the eigenvalue problem resulting from the normal mode analysis of equations (19)–(22). It is to be noted that the complex rate of growth s, which depends on σ, Ra, Pr and k, corresponds to that of the most unstable mode and, thus, the asymptotic results of the direct simulation implemented in this study provide information on the most unstable mode only. Numerical results show that, for the present problem, s is real (i.e. $s_i = 0$) for $\sigma \geqslant 2.1$.

2.3. *Computational methods*

The basic flow equations (11)–(14) and the linearized disturbance equations (19)–(22) are solved numerically by employing the computational scheme described in refs. [15, 16]. The parabolic-type equations (11), (14), (19) and (22) are cast into the finite difference form using the leap-frog method of Dufort–Frankel for the diffusion and time derivative terms [17], and central differencing for the convection terms. The Poisson equations (12) and (20) are discretized by use of five-point formula, and the resulting equations are solved by the direct method of cyclic even–odd reduction [18]. At each time level, the unsteady calculation has been completely iterated to convergence, and sufficiently small time steps ($10^{-4} \leqslant \Delta t \leqslant 10^{-3}$) are used to produce time-accurate solutions. The basic flow is assumed to reach a steady state when the relative difference of each dependent variable at every mesh point becomes less than 10^{-5}.

The procedures to obtain the transition Rayleigh number for a given axial wave number k are as follows.

(1) At a properly guessed Rayleigh number, the steady two-dimensional convective flow is numerically obtained.

(2) The disturbance equations are integrated under given initial conditions, until the asymptotic exponential behavior is established. Typically, the exponential behavior is clearly seen for $t > 2.5$ (Fig. 2).

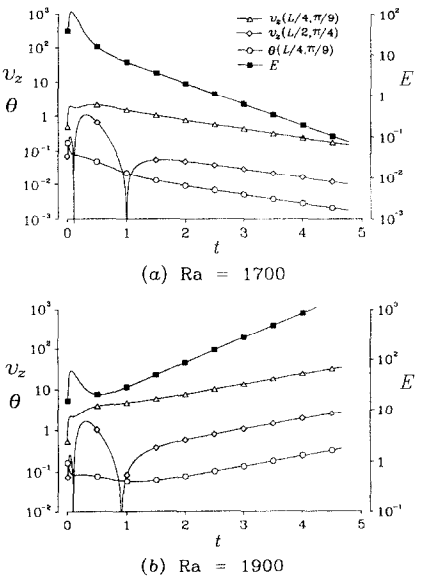

FIG. 2. Evolution of dependent variables v_z, θ and kinetic energy E for $\sigma = 5$, $k = 3.05$. (a) $Ra = 1700$, (b) $Ra = 1900$.

(3) From the exponential behavior, the rate of growth s_m for each dependent variable q_m is determined by using two successive values at a chosen point:

$$s_m = \frac{\ln (q_m^n / q_m^{n-1})}{\Delta t},$$

where the superscript n denotes the number of time steps. To ascertain that s_m is independent of choice of the location, the same calculations are performed at two other points. Typically, when $t > 3.0$, the growth rate s_m converges to one and the same constant within 0.5% relative error for all points and dependent variables examined (Fig. 2).

(4) If the absolute value of s is less than 10^{-5}, the given Rayleigh number is taken as the transition Rayleigh number. If not, another Rayleigh number is chosen and the procedures (1)–(3) are repeated. Having determined the growth rates $s^{(1)}$ and $s^{(2)}$ for Rayleigh numbers $Ra^{(1)}$ and $Ra^{(2)}$, the Rayleigh numbers for the next calculation is chosen by

$$Ra = Ra^{(2)} - \frac{s^{(2)}(Ra^{(2)} - Ra^{(1)})}{s^{(2)} - s^{(1)}}.$$

For most cases, four or five iterations give a sufficiently accurate value of the transition Rayleigh number.

Approximate values of the critical Rayleigh Ra_c and the critical wave number k_c for a given σ are determined from the minimum of the quadratic interpolation polynomial constructed from three pairs of wave number and the transition Rayleigh number (Fig. 4). The critical values remain unchanged after one iteration or two.

Calculations of both the basic flow and disturbance equations are based on the same grid system. Although the optimal grid system may depend on Ra, σ and k, a uniform $(40 \times 128)(r,\phi)$ mesh for the entire annular region $(0\text{–}2\pi)$ is found to be adequate from grid dependency tests for three gap widths, the results of which are given in Table 1. The results listed in Table 1 coincide within relative error of 0.5% and show more sensitive dependency on r-grid compared with ϕ-grid.

Table 1. Grid dependency test

Gap ratio	Grid (r, ϕ)	Ra
$\sigma = 3$	30×64	1987.2
$(k = 3.12)$	30×128	1985.7
	40×64	1998.1
	40×128	1996.8
	40×256	1996.5
	50×64	2003.1
	50×128	2001.8
	50×256	2001.5
$\sigma = 5$	30×128	1793.1
$(k = 3.12)$	30×256	1792.1
	40×128	1801.0
	40×256	1800.5
	50×128	1805.3
$\sigma = 8$	30×128	1734.7
$(k = 3.00)$	30×256	1733.0
	40×128	1742.8
	40×256	1741.3

The computations were performed on a CRAY-2S supercomputer. Determination of the critical Rayleigh number for a given gap width required a total CPU time of about 1 h, but the amount of CPU time increased considerably for σ larger than 8.5.

3. COMPUTATIONAL RESULTS AND DISCUSSION

Computations were performed over a range of relative inverse gap ratio, $2.0 \leqslant \sigma \leqslant 10$, for air $(Pr = 0.71)$.

Each successive basic flow calculation was carried out using the previously obtained steady solution as an initial guess. For disturbance equations, several initial conditions were used:

$$v_r = f_r(r)\cos(\phi - \alpha)$$

$$v_\phi = f_\phi(r)\sin(\phi - \alpha)$$

$$v_z = -\frac{1}{kr}\left(\frac{\partial (r v_r)}{\partial r} + \frac{\partial v_\phi}{\partial \phi}\right)$$

$$\theta = (r - r_i)(r - r_o)\cos(\phi - \alpha),$$

where we have chosen $\alpha = 0$ or $\pi/4$, and quadratic or quartic polynomials satisfying no-slip conditions as $f_r(r)$ and $f_\phi(r)$. Final results are independent of the initial conditions and reveal the exact symmetry about the vertical plane through the axis of cylinders, although the computational domain is the entire annulus $(0 \leqslant \phi \leqslant 2\pi)$ and initial conditions are asymmetric for $\alpha = \pi/4$.

Figure 2 illustrates typical temporal variations of disturbances for Rayleigh numbers above and below the transition Rayleigh number at a given axial wave number $(k = 3.05)$ for $\sigma = 5$. Regardless of the location and initial condition examined, disturbances increase (decrease) monotonically except for early stages $(t \leqslant 2.0)$. Moreover, the influence of the initial condition vanishes in a short transient period $(t < 0.1)$ and, hence, the evolutions of disturbances show nearly the same behavior regardless of initial conditions. Interpretation of the result according to equation (24) gives the growth (decay) rate of the most unstable (least stable) mode $s_r = 0.573$ (-0.586) with $s_i = 0$. Monotone exponential behaviors at sufficiently long times are always observed for $\sigma \geqslant 2.1$. For $\sigma = 2$, the disturbances decrease in an oscillatory manner even at $Ra = 10^5$. From Fig. 3, in which the time variations of disturbances at $Ra = 2.5 \times 10^4$ are shown, decay rate and frequency of the least stable mode are estimated as $s_r = -1.055$, $s_i = 60.9$. In Figs. 2 and 3, overall kinetic energy of disturbance over an axial period $(2\pi/k)$

$$E = \frac{\pi}{k}\int_{r_i}^{r_o}\int_0^{2\pi}\frac{1}{2}(v_r^2 + v_\phi^2 + v_z^2) r \, dr \, d\phi \qquad (25)$$

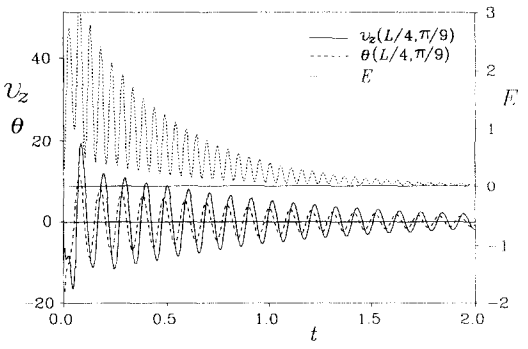

FIG. 3. Evolution of dependent variables v_z, θ and kinetic energy E for $\sigma = 2$, $k = 3.3$, $Ra = 25000$.

is also shown as a function of time. The plots presented in Fig. 2 suggest that the perturbed velocity and temperature fields evolve exponentially with the same growth rate and frequency ($=0$) independent of the location after elapsing a sufficiently long time. It may, therefore, be concluded that *the principle of exchange of stabilities* is valid for $\sigma \geqslant 2.1$ (i.e. $s_i = 0$).

In Fig. 4, neutral curves above which the flow is unstable with respect to three-dimensional disturbances are depicted for $\sigma = 2.5$ and 10.0. For $\sigma = 2.5$, the minimum critical Rayleigh number Ra_c and the critical axial wave number k_c are found to be 2195.6 and 3.106, respectively. For $\sigma = 10$, from numerical results for two-dimensional steady basic flow, it was seen that the unicellular flow prevails for the Rayleigh number less than about 2300 and the bicellular for $Ra > 2900$ and that between these two limits both patterns are possible according to initial conditions. The present results on basic flow are in excellent agreement with those reported in ref. [9].

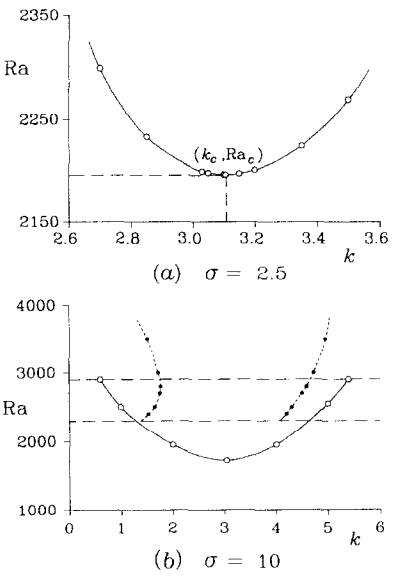

FIG. 4. Neutral stability curves; (a) $\sigma = 2.5$, (b) $\sigma = 10$. Between horizontal dashed lines both unicellular and bicellular basic flows are possible.

The neutral curve for each basic flow is shown in Fig. 4(b): solid line for unicellular basic flow and dashed for bicellular flow. As seen in the figure, the bicellular flow is always unstable with respect to a three-dimensional disturbance with the axial wave number in the range $1.8 < k < 4.2$. Fant *et al.* [9] have argued that the transition to multicellular convection from unicellular flow in a narrow gap is caused by the thermal instability between horizontal parallel planes. If this argument is admitted, the result that the bicellular flow is always unstable may be not unreasonable, since the instability in the present study can also be regarded as of thermal types.

Figure 5 displays the disturbance velocity fields at Rayleigh number higher than the critical. In the figure, the left half of the annulus presents the vector plot of r, ϕ-components of disturbance velocity and the right half the contour levels of z-component. It is seen that the disturbances are energetic in the top region of the annulus, which implies the instability is mainly caused by buoyancy effects. When the basic flow is bicellular, however, the energetic region moves towards the boundary between the counter-rotating eddies as the Rayleigh number increases (Fig. 5(c)).

Figures 6 and 7 plot the critical Rayleigh number and the critical axial wave number as a function of inverse gap width σ. The critical Rayleigh number obtained from the present calculations shows fairly good agreement with the experimental results. Rao *et al.* [8] carried out numerical calculations of three-dimensional spiral flow for $Pr = 5000$ and $\sigma = 4.7$ and reported that the spiral flows are observed at Rayleigh numbers above 2700. It is reasonable that our re-

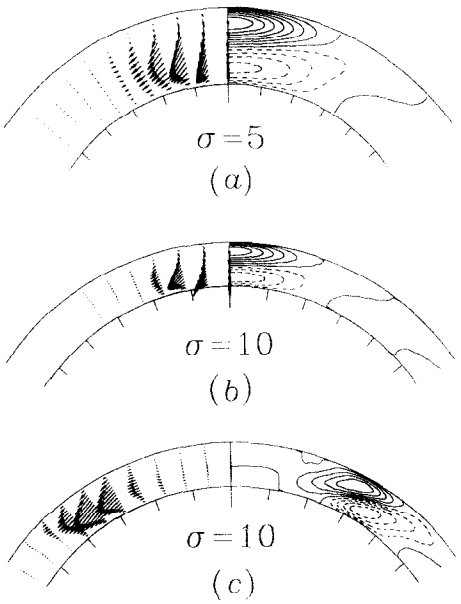

FIG. 5. Three-dimensional disturbance velocity distribution. Dashed lines represent negative contours. (a) $\sigma = 5$, $Ra = 1900$, (b) $\sigma = 10$, $Ra = 2500$, basic flow is unicellular, (c) $\sigma = 10$, $Ra = 3000$, basic flow is bicellular. For all cases, $k = 3.05$.

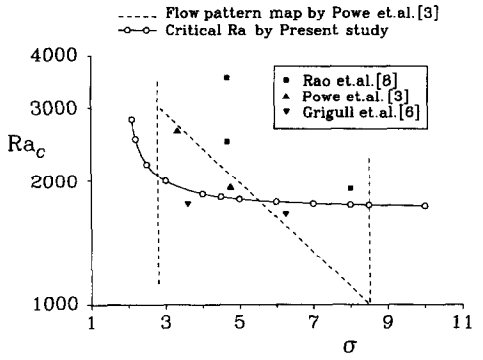

FIG. 6. Critical Rayleigh number Ra_c as a function of σ. Some experimental results are also shown; after Powe *et al.* [3], Grigull *et al.* [6], Rao *et al.* [8]. Dashed line denotes the transition curve to 3-D flow suggested by Powe *et al.* [3].

sults show a lower critical Rayleigh number than Rao *et al.*'s, since the present analysis calculates the Rayleigh numbers at which instability manifests and these values are presumably lower than those found by experiments. The figure shows that instability due to a three-dimensional disturbance occurs even in the region $2.1 \leqslant \sigma < 2.8$, which has been designated as a two-dimensional oscillatory regime by Powe *et al.* [3]. For $\sigma \leqslant 3$, the critical Rayleigh number Ra_c as well as the critical wave number k_c increases abruptly as σ decreases. On the other hand, in the region $\sigma \geqslant 3$ (spiral flow regime), Ra_c and k_c vary slowly as σ increases. To the best of the present authors' knowledge, no work reports explicitly the information on axial wave number of three-dimensional natural convection in a horizontal annulus. From Fig. 11 of Rao *et al.* [8] which plots the isotherms on the vertical symmetry plane for $\sigma = 4.7$, $Ra = 2700$ and $Pr = 5000$, we can estimate roughly the axial wave number as 3.14. For the same inverse gap ratio, the present study gives the critical wave number 3.05, which shows both results are in good agreement despite the difference in Prandtl numbers.

Although quantitative investigations of the spiral flow above the critical Rayleigh number require the analysis of three-dimensional full Navier–Stokes equations, the disturbed velocity distribution of the most unstable mode can provide qualitative features of the flow slightly above Ra_c, since only the most unstable mode grows exponentially and all other modes decay. The exponential growth of the most unstable mode will be altered by the nonlinear terms in the Navier–Stokes equations and eventually the amplitude of disturbances may settle at a finite value [12];

$$\text{Amplitude} \propto (Ra/Ra_c - 1)^{1/2} \quad \text{as } Ra \downarrow Ra_c.$$

The plot of a superposition of the form $\mathbf{V}_s(r, \phi) + \varepsilon \mathbf{v}_p(r, \phi, z)$ will, thus, provide a help to get a first insight about the spatial structure of the spiral flow when Ra slightly exceeds Ra_c. In Fig. 8, we have arbitrarily chosen $\varepsilon = 0.3$. The figures show that except for the top region, in which three-dimensional flow structures are seen, the flow is nearly two-dimensional. The fact that the fluid particle paths and iso-

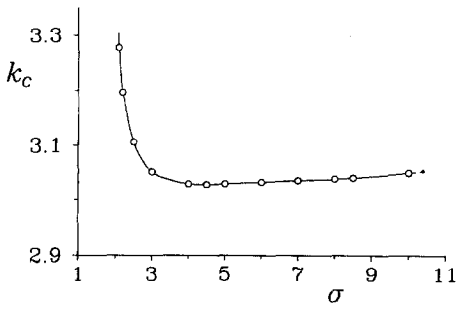

FIG. 7. Critical wave number k_c as a function of σ.

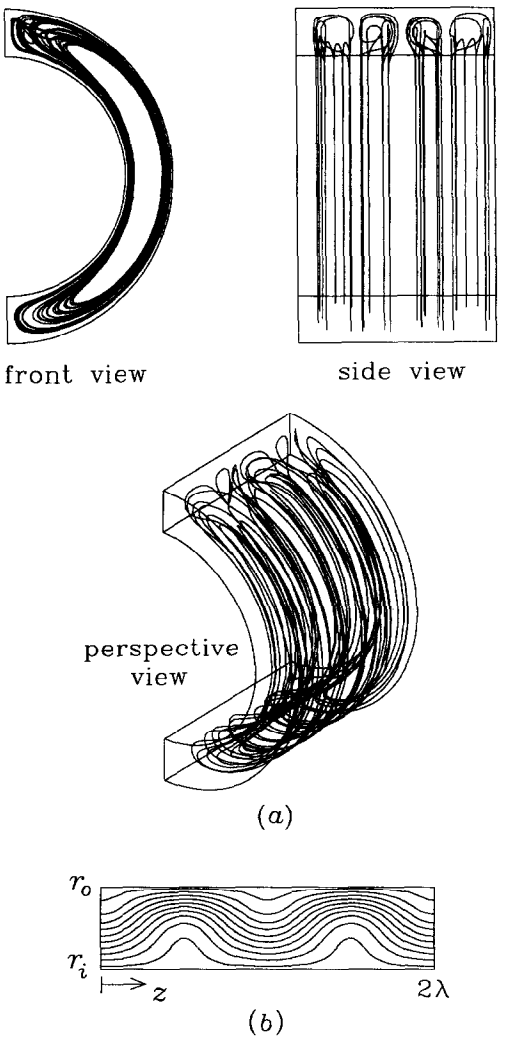

FIG. 8. Fluid particle paths and isotherms on the vertical symmetry plane for $\sigma = 5$, $k = 3.05$, $Ra = 1900$. (a) Particle paths, (b) isotherms. Wave length $\lambda = 2\pi/k$.

therms on the vertical symmetric plane are similar to those calculated by Rao *et al.* [8] reinforces the assumption that the basic flow and the most unstable mode can provide features of the flow at a Rayleigh number slightly above Ra_c.

4. CONCLUSIONS

Stability of two-dimensional natural convective flow between two concentric horizontal cylinders against infinitesimal three-dimensional disturbances is investigated for a fluid of Prandtl number 0.71 (air). The linearized disturbance equations are integrated numerically to obtain the most unstable (least stable) mode.

In the range of $2.1 \leqslant \sigma \leqslant 10.0$, the critical Rayleigh number above which the basic flow is unstable is determined as a function of the relative inverse gap ratio σ. Experimentally observed results on the transition to spiral flow [3] shows good agreement with those obtained from stability analysis. It is found that *the principle of exchange of stabilities* is valid and that the disturbances are energetic in the top region of the annulus, which implies that the instability mainly results from the buoyancy effects. It is inferred that the spiral flows at Rayleigh numbers slightly greater than the critical Rayleigh number will show three-dimensional characteristics in the top region of the annulus and remain nearly two-dimensional in other regions.

Acknowledgement—The authors gratefully acknowledge the support from AFERC (Advanced Fluid Engineering Research Center).

REFERENCES

1. T. H. Kuehn and R. J. Goldstein, An experimental and theoretical study of natural convection in the annulus between horizontal concentric cylinders, *J. Fluid Mech.* **74,** 695–719 (1976).
2. D. B. Fant, J. Prusa and A. P. Rothmayer, Unsteady multicellular natural convection in a narrow horizontal cylindrical annulus, *ASME J. Heat Transfer* **112,** 379–387 (1990).
3. R. E. Powe, C. T. Carley and E. H. Bishop, Free convection flow patterns in cylindrical annuli, *ASME J. Heat Transfer* **91,** 310–314 (1969).
4. E. H. Bishop, C. T. Carley and R. E. Powe, Natural convective oscillatory flow in cylindrical annuli, *Int. J. Heat Mass Transfer* **11,** 1741–1752 (1968).
5. C. Liu, W. K. Mueller and F. Landis, Natural convection heat transfer in long horizontal cylindrical annuli, *International Developments in Heat Transfer*, Part V, pp. 976–984 (1961).
6. U. Grigull and W. Hauf, Natural convection in horizontal cylindrical annuli, *Proc. 3rd Int. Heat Transfer Conf.*, Vol. 2, pp. 182–195 (1966).
7. U. Grigull and W. Hauf, Authors rebuttal, *Proceedings of the Third International Heat Transfer Conference*, Vol. 6, pp. 157–158, Am. Inst. Chem. Engrs. New York (1967).
8. Y. F. Rao, Y. Miki, K. Fukuda, Y. Takata and S. Hasegawa, Flow patterns of natural convection in horizontal cylindrical annuli, *Int. J. Heat Mass Transfer* **28,** 705–714 (1985).
9. D. B. Fant, A. Rothmayer and J. Prusa, Natural convective flow instability between horizontal concentric cylinders, *J. Thermophys. Heat Transfer* **5,** 407–414 (1991).
10. Y. Takata, K. Iwashige, K. Fukuda and S. Hasegawa, Three-dimensional natural convection in inclined cylindrical annulus, *Int. J. Heat Mass Transfer* **27,** 747–754 (1984).
11. K. Vafai and J. Ettefagh, An investigation of transient three-dimensional buoyancy-driven flow and heat transfer in a closed horizontal annulus, *Int. J. Heat Mass Transfer* **34,** 2555–2570 (1991).
12. P. G. Drazin and W. H. Reid, *Hydrodynamic Stability*, Cambridge University Press, New York (1981).
13. K. Aziz and J. D. Hellums, Numerical solution of the three-dimensional equations of motion for laminar natural convection, *Phys. Fluids* **10,** 314–324 (1967).
14. G. J. Hirasaki and J. D. Hellums, A general formulation of the boundary conditions on the vector potential in three-dimensional hydrodynamics, *Quart. J. Appl. Math.* **26,** 331–342 (1968).
15. J.-S. Yoo and M.-U. Kim, Two-dimensional convection in a horizontal fluid layer with spatially periodic boundary temperatures, *Fluid Dyn. Res.* **7,** 181–200 (1991).
16. J.-S. Yoo, J. Y. Choi and M.-U. Kim, Multicellular natural convection of a low Prandtl number fluid between horizontal concentric cylinders, *Numer. Heat Transfer* (in press).
17. P. J. Roache, *Computational Fluid Dynamics*, Hermosa, Albuquerque, New Mexico (1976).
18. B. L. Buzbee, G. H. Golub and C. W. Nielson, On direct methods for solving Poisson's equations, *SIAM J. Numer. Anal.* **7,** 627–656 (1970).